Higher harmonic generation of guided waves at delaminations in laminated composite beams

Reza Soleimanpour[1], Ching-Tai Ng[1,*] and Chun Wang[2]

Abstract: Detection and characterization of delamination damage is of great importance to the assurance of structural safety. The present work investigates the potential of a baseline-free structural health monitoring technique based on higher harmonics resulting from the nonlinear interaction of guided wave and a delamination. The nonlinearity considered in this study arises from the clapping of the sub-laminates in the delaminated region, which generates contact acoustic nonlinearity (CAN). Both explicit finite element (FE) simulations and experimental tests are conducted on composite laminates containing a delamination of different sizes and at different through-thickness locations. The results show that the interaction between the fundamental asymmetric mode (A_0) of guided wave and a delamination generates CAN in the form of higher harmonics, which provides a good measure for identifying the existence of delaminations and determining their sizes in laminated composite beams. This new

[1] School of Civil, Environmental & Mining Engineering, The University of Adelaide, SA, Australia

[2] School of Mechanical and Manufacturing Engineering, University of New South Wales (UNSW), Sydney, Australia

Corresponding author:

* Ching-Tai Ng, School of Civil, Environmental & Mining Engineering, The University of Adelaide, SA, Australia

Email: alex.ng@adelaide.edu.au

insight into the generation mechanisms of nonlinear higher order harmonics in composite laminates will enhance the detection and monitoring of damage in composite structures.

Keywords

Contact acoustic nonlinearity, delamination, fiber reinforced laminated composite beam, finite element, nonlinear guided waves.

Introduction

Damage detection is essential to structural integrity management of engineered structures on which human safety depends. Structural health monitoring techniques employing guided waves and distributed sensors have shown promises in complementing existing non-destructive evaluation (NDE) techniques, such as radiography, electro-mechanical impedance based, eddy current technique, visual inspection, shearography, thermography and conventional ultrasonic [1]. Compared to conventional NDE techniques, guided waves techniques [2-4] offer several major advantages, such as the ability to inspect inaccessible locations and large areas autonomously, without interrupting operations [5-9]. However, guided wave methods require subtracting the wave data of the un-damaged state (baseline data) from the total wave to obtain the scattered wave data attributed to damage [10,11]. Recently nonlinear ultrasonic phenomenon is emerging as a new concept to alleviate the need for baseline data by exploiting side bands and higher harmonics that are generated only by the clapping and/or friction between the faces of a crack subjected to an incident wave.

When a single-frequency guided wave encounters a linear structural feature, such as a hole or a stiffener, the scattered waves is of the same frequency as the original wave. However, additional frequencies can be generated by geometrically nonlinear structural features such as breathing cracks whose surfaces come into contact [12], or material nonlinearity [13,14]. Examples of these nonlinear acoustical phenomena include (a) higher harmonic generation, (b) sub-harmonic generation, (c) nonlinear resonance and (d) mix frequency response. Among these, higher order harmonic generation and frequency mixing have been commonly used as indicators of acoustic nonlinearities.

Basically the non-linear acoustic phenomena involve classical and non-classic responses. The classical non-linear response is mostly concerned with material imperfections such as intrinsic nonlinearities due to imperfections in atomic lattices leading to higher harmonic generation. Localized fatigue cracks, distributed micro-cracks or other material imperfections are some of the sources of classical non-linear response. Research work in this area also involves higher harmonic generation of Lamb waves used for the detection of material nonlinearity and damage.

Classical nonlinear effects in guided waves propagation have been investigated by many researchers and explored for damage detection. Deng [15,16] investigated the generation of second harmonic of shear horizontal waves and Lamb waves in metallic plates. Müller et al. [17] investigated the characteristics of second harmonic generation of Lamb wave in a plate with quadratic nonlinearity. Liu et al. [13] investigated the symmetry properties of second harmonic Lamb waves by examining anti-symmetric Lamb mode pairs. Zhang et al. [18] reported the observation of cumulative second harmonic generation of Lamb wave in long bones based on the modal expansion

approach to waveguide excitation and the dispersion characteristics of Lamb waves in long bones. It was shown that the second-harmonic signal generated by fundamental Lamb waves in long bones is observed clearly, and the effect is cumulative with propagation distance when the fundamental Lamb wave mode and its second harmonic mode have the same phase velocities. Xiang et al. [19] developed an analytical model for the effect of the interactions of dislocations with precipitate coherency strains on the generation of second harmonic of Lamb waves in metallic alloys. Lissenden et at. [20] studied generation of higher harmonics of guided waves in aluminum plates with plastic deformation. It was shown that plastic deformation has a significant effect on the harmonic amplitude ratio. Pruell et al. [21] studied the generation of nonlinear guided waves by fatigue crack in metallic plates. It was shown that the phase and group velocity matching is essential for practical generation of nonlinear guided waves. A technique was developed for quantitatively assessing fatigue damages in metallic plates based on nonlinear guided waves. Bermes et al. [22] developed a procedure to determine the second harmonic of the Lamb waves in metallic plates. Srivastava and Lanza di Scalea [23] theoretically studied the symmetry characteristics of Rayleigh–Lamb guided waves in nonlinear, isotropic plates. It was shown that antisymmetric motion is prohibited at all the higher order even harmonics whereas all the higher order odd harmonics allow both symmetric and antisymmetric motions.

In contrast to classical nonlinear response, the non-classical non-linear response mostly arises in contact-type defects in material. Crack-wave interactions that exhibit vibro-acoustic modulations, sub-harmonic generation or stress-strain hysteresis are some of the sources of non-classical nonlinear responses.

For a tight crack without any gap between its faces, its surfaces will close under compressive stress, thus allowing the compressive part of the wave to propagate through unimpeded. The tensile part of the wave, however, will open the crack, thus causing scattering, as shown in Fig. 1. Therefore, a tight crack effectively behaves like a half-wave rectifier. When the crack surfaces come into contact, the dynamic pressure between crack faces generates additional waves approximately twice the frequency of the original wave, or nonlinear waves in the form of higher harmonics. Since higher harmonics are induced only by contacting surfaces such as cracks, their presence, which can be identified directly from the total wave field without the need for accurate baseline data, offer a new route for baseline free damage detection or structural health monitoring.

Fig.1 Interaction of an incident wave with a crack

Two non-classical nonlinear mechanisms are possible due to the interaction of crack surfaces with a propagating incident wave. The first one is referred to as clapping, which is generated due to asymmetry in stress-strain characteristics for damaged interfaces causing the stiffness of the materials to be higher in compression but lower in tension. This asymmetric variation in local stiffness will distort the wave pattern and results in wave nonlinearity in the form of higher even harmonics of the incident wave frequency. The friction between damage interfaces when they slip causes symmetric change in local stiffness, which results in the generation of higher odd harmonics. Awrejcewicz and Olejnic [24], Pecorari and Solodov [25], carried out comprehensive studies on the effect of this second type of mechanism for wave nonlinearity.

Nonlinear analysis methods focusing on non-classical nonlinear behavior of interfaces are referred to as local nonlinearities, which have attracted increasing interest in theoretical and applied research in the past few years [26,27]. Kim *et al*. [28] developed a nonlinear model for investigating the CAN of a closed crack in aluminum plate in order to analyze the nonlinear characteristics of the transmitted waves. These studies have found that the interfacial stiffness has a significant effect on the amplitude of the resultant second order harmonic. The experimental results showed that the amplitude of the second order harmonic correlates with the crack closure process, in agreement with numerical results. Recently, Hong *et al*. [29] investigated the phenomenon of CAN related to breathing fatigue cracks and material nonlinearity using a piezoelectric sensor network. It was shown that the relative acoustic nonlinearity parameter increases proportionally with the wave propagation distance due to the geometric and materials nonlinearities. Solodov *et al*. [30] investigated the acoustic wave interaction with non-bonded contact interfaces (crack) in solids through experiments and simulations. It was shown that changes in the interface stiffness characteristics are the major cause of CAN. The stiffness parametric modulation and instability of oscillations are due to the asymmetry in the contact restoring forces, which results in the generation of sub-harmonics. It was concluded that sub-harmonics and higher harmonics are good indicators for the existence of defects in metallic structures.

A recent study was reported by Kishiwada *et al*. [31] on using the fundamental antisymmetric mode (A_0) Lamb wave for detecting clapping actions between two thin aluminum plates under different pressures at the contact interface. The study showed that clapping between two aluminum plates generates higher harmonics especially odd harmonics of Lamb wave. Moreover, the applied pressure affects the dispersive

behavior of asymmetric Lamb waves. It was concluded that the phenomena of generation odd harmonics due to clapping effect could be used for damage detection and imaging.

More advanced non-classical nonlinear response techniques such as modulation methods were invented by Korotkov et al. [32] and Donskoy et al. [33] which involved both classical and non-classical nonlinear responses and exploited the effects of the nonlinear interaction between ultrasonic probing signal and a low frequency vibration for damage detection.

To date, most of the studies on non-classical responses of nonlinear ultrasonic have focused on isotropic materials. Very limited research has been reported on the generation of nonlinear guided waves by delaminations in composite laminates [34,35]. Here we present an experimental and computational investigation of the interaction between narrow-band guided waves with delamination craks, with a view of using of nonlinear guided waves for detecting delamination damage in fiber reinforced composites.

This paper is organized as follows. The first section describes the experimental method to characterise the propagation behaviour of guided waves, including group and phase velocity, attenuation constants and nonlinear wave measurement. The second section describes computational simulations using three-dimensional (3D) finite element (FE) method for both the propagation and generation of non-linear guided waves, taking into account of the effect of attenuation. Verification of the FE model is then provided in the third section, which consists of linear and nonlinear guided wave verification. The forth

section presents a validation of the FE model by comparing the simulated results with experimental data. The effect of material damping is modeled using Rayleigh damping coefficients. In the sixth section a comprehensive study of the nonlinear guided wave at delamination in laminated composite beam is carried out using the FE model, especially for delamination of varying size relative to the wavelength of the incident wave and at different through-thickness locations in the laminate. In addition, the effect of damping on the nonlinear guided wave is also discussed. Finally conclusions are presented together with opportunities for future research.

Experimental Details

The experiments described in this section were carried out to verify the 3D FE models that will be employed to simulate the propagation of both linear and non-linear guided waves. The linear guided waves verification was carried out in order to confirm the model parameters for the guided waves obtained from FE simulation, by matching the phase and group velocity with the analytical dispersion curves. The non-linear guided waves verification was carried out in order to ascertain the non-linear guided waves parameters such as higher harmonics induced by contact acoustic non-linearity by comparing acquired data from both approaches in frequency domain.

Specimens

For experimental validation of the FE models, specimens were manufactured from eight plies of VTM264 unidirectional carbon/epoxy prepreg with a stacking sequence of $[0/90/0/90]_S$. This cured lamina has a fibre volume fraction of 0.55, with density and thickness being 1538 kg/m^3 and 0.2 mm respectively. The elastic properties of the lamina are shown in Table 1.

Table 1: Elastic properties of the VTM264 prepreg lamina

The dimension of the composite beams is 285 mm × 12 mm × 1.6 mm. One specimen was intact for verification of the performance of 3D FE models in predicting the linear guided wave propagation. The other specimen had a 15 mm long delamination located between the third and fourth plies, as schematically shown in Fig 2. Two very short Teflon films were first inserted between the third and fourth ply of the composite laminate during the manufacturing process. To break the weak bonding between the composite and the Teflon films, the specimen was subjected to a three-point bending until a delamination formed and grew to a size slightly larger than the Teflon insert.

Fig. 2 Schematic diagram of a composite beam specimen with delamination and its cross section

Experiment setup for validation of linear guided waves

A 12 mm × 6 mm × 2 mm rectangular piezoceramic transducer was adhesively bonded to one end of the beam to excite the A_0 guided wave. A 3 mm thick brass backing mass was used to increase the excitability of the A_0 guided wave. The excitation pulse was generated by a computer controlled signal generator with a 10 V peak-to-peak output range, which was further amplified to 50 V peak-to-peak output voltages using an amplifier. The out-of-plane displacements were measured by using a scanning laser Doppler vibrometer (Polytec PSV-400-3D-M) and the data was sent to the laser controller and data acquisition system for post-processing. A band-pass filter was introduced to the system and the average of signals was calculated over 1000 repeats of

acquisitions to improve the signal-to-noise ratio. Fig. 3 shows the experiment setup used in this study.

Fig. 3 Experiment setup used for verification of FE models

This study employed a 5-cycle sinusoidal tone burst pulse modulated by a Hann window. The centre frequency of the tone burst was swept from 20 kHz to 300 kHz at 20 kHz increments and the phase velocity and group velocityof the wave at each excitation center frequency was calculated [11,36, 37] and the wave phase and group velocity dispersion curves for both approaches were plotted and compared accordingly.

Determination of material damping in laminated composite beams

To account for material damping on the propagation of guided wave, a 5-cycle sinusoidal tone burst pulse modulated by Hann window with central frequency of 140 kHz was applied on the intact laminated composite beam. Although there are no certain criteria on the selection of the excitation frequency, an appropriate frequency is considered to be able to achieve good signal-to-noise ratio, smaller wave dispersion, a small number of co-existing wave modes, and also high sensitivity to damage. In this study, the optimum excitation frequency was obtained through experimentation. A couple of frequencies within the range of 50 kHz to 200 kHz were examined. Since 140 kHz showed the best signal to the noise ratio, this frequency was used for the rest of study. The maximum magnitude of the out-of-plane displacement was captured at 19 measurement points, at a spacing of 10 mm, located between 20 mm to 200 mm away from the actuator.

The attenuation coefficient (k_i) is determined by curve-fitting the following relationship with the attenuation data [38] shown in Fig.4:

$$\frac{\mathrm{A}(\Delta x)}{A_0} = \exp(k_i \Delta x) \tag{3}$$

where A_0 and $A(\Delta x)$ are the signal amplitudes at a reference point and at distance Δx away from the reference point, respectively. The attenuation curve was plotted by finding the best exponential fit to experimental results and is shown in Fig. 4. The value of k_i for the laminated composite beam employed in this study is 3.1 1/m.

Fig. 4 Attenuation of A_0 guided wave in composite structure at 140 kHz

Based on the attenuation coefficient, the Rayleigh mass proportional and stiffness proportional damping constants can be calculated from the following equations [38]:

$$\alpha_\omega = 2k_i C_g \tag{4}$$

$$\beta_\omega = \frac{2k_i C_g}{\omega^2} \tag{5}$$

where α_ω and β_ω are the mass proportional and stiffness proportional damping constants, C_g is the group velocity, and ω is the angular central frequency of the tone burst wave. Estimated group velocity of the asymmetric guided waves at 140 kHz is 1401 m/s. Therefore, the values of $\alpha_\omega$and β_ω at frequency of 140 kHz are calculated as 8730 rad/s and 1.128×10^{-8} rad/s, respectively. These constants will be implemented in the FE models to account for the effect of material damping in the composite beams.

Experiment setup for validation of non-linear guided waves

Two rectangular piezoceramic actuators (12 mm × 6 mm × 2 mm) were adhesively attached to the delaminated beam at 107.5 mm from each beam end. The excitation signal was generated by a computer controlled arbitrary waveform generator (NI PXI-5412) with 10 V peak-to-peak output voltage and then amplified by an amplifier with peak-to-peak voltage of 50 V. The response of the receiver transducer was recorded by NI PXI-5105 digitizer for further post-processing. Fig. 5 shows the experiment setup used in this study.

Fig. 5 Excitation and acquisition of higher harmonic waves

Computational modelling of guided waves in composite laminate

In this study, a 3D explicit FE method [39] was used to simulate the propagation of guided wave in cross-ply laminated composite beams. In the FE model, each lamina was modelled using a layer of eight-noded 3D fully integrated linear solid elements with incompatible modes (C3D8I) with hourglass control. The incompatible modes have added internal degrees of freedom that improve the representation of bending in the interior of the element. Stewart *et al*. [44] recommended limiting the hourglass energy to less than 2% of the total energy to ensure the accuracy of predicting the guided wave propagation in solids and this was implemented in all FE models throughout this study. Each node of the solid brick element has three translational degrees-of-freedom (DOFs). To ensure the numerical stability and to simulate the damping effect of composite

materials, the FE models incorporate Rayleigh mass proportional and stiffness proportional damping discussed in the previous section [45].

The A_0 guided wave was excited by applying out-of-plane nodal displacements to surface nodes located at one end of the beam, which simulates a piston type excitation generated by a 12 mm × 6 mm rectangular transducer [46]. Fully integrated linear solid elements with incompatible modes (C3D8I) having in-plan dimensions of 0.4×0.4 mm^2 and 0.2 mm thickness were used in the beam models, as it has been shown that this element type with an aspect ratio of 2 is suitable for simulating the propagation of guided waves at delaminations in composite laminates [39]. Packo et al [40] investigated simulation of propagation of guided waves in isotropic and anisotropic plates. It was shown that for simulation of propagation of fundamental and first-order modes of Lamb waves in anisotropic plates a typical 4-8 number of elements per ply of material provides the perfect results. However, other studies [41, 42, 43] show that one element per ply still can predict the propagation of Lamb waves in composite beams and plates with good accuracy when the incident frequency is below the cut off frequency of second mode. In this study, to reduce the computational expenses each lamina was modelled using one element per ply. The dynamic simulation was solved by the explicit FE code in ABAQUS v6.14, which uses the central-difference integration [47]. In this scheme, the integration operator matrix is inverted and a set of nonlinear equilibrium equations is solved at each time increment. Since the central different integration scheme is conditionally stable, the increment time step has to be small enough to ensure the stability. In this study the increment time step is automatically calculated by ABAQUS.

In the FE model, CAN is simulated by applying frictionless surface-to-surface contact interaction (friction coefficient is set to be zero) to avoid interpenetration of the delamination surfaces during the wave propagation. Direct Enforcement Method was used to maintain the pressure-penetration relationship through Lagrange multiplier method. By applying the direct enforcement condition in variational formulation for a steady-state analysis [47], we get

$$\delta \prod^{c} = \delta p h + p \delta h \tag{6}$$

where $\delta \prod^{c}$ is the contact virtual work contribution, p is the Lagrangian multiplier, and h is the overclosure.

Hard contact was used in FE simulation. For Hard Contact, the definition of the contact pressure between two surfaces at a point, p, as a function of the overclosure of the surfaces or the interpenetration of the surfaces (h) is

$p = 0$ for $h < 0$ surfaces are not in contact

$h=0$ for $p>0$ surfaces are contacting

Material damping was applied in FE simulation using experimentally obtained Rayleigh mass and stiffness proportional damping constants; the values are presented in the following section. The scattered wave $w_s(t)$ is determined by subtracting the baseline data $w_b(t)$ from the total wave $w_t(t)$. In terms of the Fourier transform, this can be expressed as

$$\widehat{w_s}(f_c) = \widehat{w_t}(f_c) - \widehat{w_b}(f_c) \tag{6}$$

By comparison, the second harmonics $\widehat{w_h}(2f_c)$ can be directly determined from the total field, because it is not present in the baseline,

$$\widehat{w_h}(2f_c) = \widehat{w_t}(2f_c) \tag{7}$$

The excitation signals in both the FE simulation and the experiment are a narrow-band tone burst in the form of an 8-cycle sinusoidal signal modulated by a Hann window with a central frequency of 140 kHz. Fig. 6 shows a snapshot of the computational results of the interaction of A_0 guided wave with the delamination in the laminated composite beam.

Fig. 6 A typical contour snapshot of FE simulated out-of-plane displacement of guided wave in composite beam with a delamination (time = 128.9 μs. Scale factor = 250)

Results and discussions

Linear guided waves

In this section, an experimental verification of linear wave propagation in fibre reinforced laminated composite beam FE model is presented. The experimental verification is carried out using the phase and group velocity dispersion curve comparison for fundamental asymmetric guided waves. Therefore, the phase and group velocity of the incident guided waves calculated from the FE simulations and compared with the experiment data. The signal was extracted at four consecutive measurement points located 4 mm away from each other and the first measurement point was 100 mm from the excitation location. Since the first measurement location is away from the

excitation more than four times of the wavelengths, the evanescent waves are negligible in the measurements. The captured data at four measurement points were used to calculate the phase and group velocity. The simulation results are compared with the experimental results to ensure the capability of the FE model in simulating the linear guided wave propagation in laminated composite beams. Fig. 7 shows the estimated phase and group velocity dispersion curves calculated from the FE simulated and experimentally measured data.

Fig 7. Dispersion curve comparison estimated by FE and experimental results

As can be seen from Fig.7 both the phase and group velocity dispersion curves from FE solution are in good agreement with the experimentally measured dispersion curves. This confirms that the FE model is able to accurately predict the phase and group velocities of the guided wave in fiber reinforced laminated composites.

Non-linear guided waves

To reveal the higher harmonic waves, the results from experiments and computational simulation are transformed to frequency domain using the Fast Fourier transform (FFT). Figs.8a and 8b show the results measured at 70 mm from excitation point for both intact and delaminated specimens. As shown in Fig.8b, both FE simulated and experimental data contain higher frequency components with the maximum amplitude being at around 280 kHz, twice of the original incident wave frequency. By comparison, the data obtained from the intact composite beam plotted in Fig. 8a show no higher harmonic waves. As shown in Fig.8a, the FFT of the data from the intact beam only contains the

frequency components at the excitation frequency (140 kHz). However, the FFT of the experimental results shows some humps around the second harmonic for delaminated specimen. The source of these humps can be surface roughness or friction at delamination interface [48]. Since friction was not considered in the FE model, these humps do not exist in FE model results. Therefore, CAN is the major source of nonlinear waves in laminated composite beam with the delamination. These results also confirm that the FE model is capable of predicting the generation of higher harmonic waves by delamination damage.

Fig. 8 Normalized FFT of the signal obtained from the experiment and FE simulation, a) intact beam b) beam with the delamination between 3^{rd} and 4^{th} ply. The response measured at 70 mm from excitation and 35 mm from centre of delamination.

Damage case studies

To investigate the effect of delamination size on the strength of higher harmonic wave, computational simulations are performed for a range of sizes and through-thickness positions of a single delamination. The incident wave wavelength was calculated using DISPERSE software [49]. Table 2 summarizes the different sizes considered in this study, while Table 3 provides a summary of damage locations. The excitation location was at the left end of the beam and measurements were carried out at locations of 160 mm (measurement point A) and 240 mm (measurement point B) away from the left beam end which provide backward and forward scattering wave packets data, respectively. The scattered waves from the delamination were obtained by monitoring the out-of-plane displacement at the mid-thickness of the beam model. This ensures

only the A_0 guided wave is detected as the fundamental symmetric mode and shear horizontal mode of guided wave have zero out-of-plane displacement at this location.

Table 2: Damage cases according to delamination size to wavelength ratio (d/λ)

Table 3: Damage cases with different through-thickness locations of delamination

Non-linear forward scattering signals

The time-domain out-of-plane displacement obtained from the FE models (with and without considering surface contact) at measurement point B for Damage Case 3 with delamination size to wavelength ratio of 1.0 (delamination size = 8 mm, located between 3rd and 4th layers) is shown in Fig. 9. Wave distortion is observed in scattered wave signal when surface contact is modelled, while no discernible difference can be observed if surface contact is not considered. However, the wave distortion (the zoomed-in area in Fig.9), which refers to nonlinear wave, is very small and hard to observe in the time-domain signal. The FE results show that there is only minor or no nonlinearity is observed when the delamination is located between 4th and 5th layer (Damage Case 4). This is because the delamination is located symmetrically in the through-thickness direction of the beam, which causes no contact interaction between the two sub-laminates within the delamination region. Hence, no nonlinear guided wave is generated in this case.

Fig. 9 Transmitted wave response computed by finite element model for damage case study 3, $d/\lambda = 1$

Fig. 10 FFT of forward scattered wave by using baseline subtraction

To reveal the presence of higher harmonics, the time-domain signal was transformed to the frequency domain using FFT. Fig. 10 shows the normalised amplitudes of the forward scattering signals. To compare the strength of nonlinear higher harmonic wave with that of the linear wave, the scattered wave results were obtained by subtracting the responses from finite element models without and with contact condition. As shown in Fig. 10 several peaks are observed at higher frequencies in the model with contact interaction at the delamination region. In addition to the excitation frequency, second and third higher harmonics are visible in some cases. The processed data in frequency domain only reveal the existence of higher harmonics. However, to ensure that the delamination is the only source of existing humps in FFT results, the time of flight of the non-linear wave packets were calculated, as described below.

To examine the propagation time of the higher harmonics, the simulation data were transformed to the time-frequency domain using continuous Gabor wavelet transform, which simultaneously provides time-frequency information of the guided wave signals. The results in the time-frequency domain are presented in Figs. 11a and 11b, clearly showing higher harmonics. For some damage cases, the second higher harmonic wave at 280 KHz almost arrives at the same as the linear scattered wave. Nevertheless, for some other damage cases such as the case where delamination is located between 3^{rd} and 4^{th} ply, the higher harmonic wave packets arrive at a later time than the linear scattered wave. The results show that this variation in the time of arrival of non-linear wave packet is attributed to the time of initialization of clapping between delamination crack surfaces. This means that, for some damage cases, it takes a certain amount of

time until the interface initiate clapping and thus non-linear wave packets generation is delayed. As shown in Figs. 11a and 11b, higher harmonics are located between 200 μs to 225 μs. This matches the time domain results, which indicate the signal distortion occurring immediately after the arrival time of incident wave. As it is shown, the non-linear wave packets in scattered wave packets are hidden within the incident wave and sometimes those wave packets cannot be separated in time-domain acquired data. Therefore, processing the data in the frequency domain reveals more useful information regarding the existence of delamination crack.

Fig. 11 Time-frequency energy density spectrum of the forward scattered wave (after baseline subtraction) for Damage Cases 1-3 (left to right) and delamination size to the wavelength ratio of a) 0.75 and b) 1.0.

Non-linear backward scattering signals

Applying the same method used for studying the forward scattered wave, the computational results are processed to extract the backward scattered waves. Similar to the forward scattering case, the Damage Case 4 (delamination located between 4^{th} and 5^{th} layers) did not generate any discernible nonlinear waves, while the other three cases produced nonlinear waves. The time-domain out-of-plane displacements of Damage Case 3 (d/λ= 1) obtained from FE models with and without considering contact are shown in Fig. 12. The data was captured at measurement point B located at 160 mm from the left beam end. Similar to forward scattered signals, distortion is visible in the total reflected wave. However, the wave distortion is very small and hardly visible in the time-domain acquired data. In the case of measurement point being close to the excitation location, the backward scattered signal will mix with the incident wave and

the distortion may not be visible which makes the time domain data ineffective for damage detection.

Fig. 12 Reflected waves of Damage Case 3 (d/λ= 1) from FE models.

Fig. 13 shows the FFT of the extracted nonlinear backward scattered waves for all three damage cases. Several peaks are observed at higher frequencies. As shown in Figs. 14a and 14b, second harmonic at 280 kHz is visible in time-frequency energy density spectrum plots. Similar to time-frequency energy density spectrum plots of forward scattering waves, third harmonic is hardly visible in time-frequency energy density spectrum plots due to the small amplitude relative to the main reflected signal. It should be noted that the signal shown in the time-frequency energy density spectrum is obtained after the baseline subtraction, i.e. the incident wave information does not exist in the FFT and time-frequency energy density spectrum plots. The time-frequency energy density spectrum plots provide additional information about the frequency and the arrival time of each wave packet. According to the time domain data, the wave distortion is located between 180 μs to 225 μs which agrees with CTW plots showing the same time range for higher harmonics. As can be seen, the amplitude of the second harmonic varies with damage modes.

Fig. 7 FFT of nonlinear backward scattering waves extracted using baseline subtraction

Fig. 14 Time-frequency energy density spectrum of backward scattered wave (after baseline subtraction) for Damage Cases 1-3 (left to right) and delamination size to the wavelength ratio of a) 0.75 and b) 1

Comparison between the nonlinear forward and backward scattering waves

Delamination has been found to generate stronger forward scattering than backward scattering [10]. To examine the effect of damage size on the nonlinear scattered wave, with a view of developing appropriate damage detection method, a comparison of the normalized amplitude of the backward and forward higher harmonics are presented in Figs. 15a-15c. The captured data at each measurement point were normalized to the amplitude of incident wave at the same measurement points in intact model. It can be seen that Damage Case 2, where the delamination located between 2^{nd} and 3^{rd} layer, has the maximum magnitude of second harmonic. Moreover, the amplitude of the second harmonic for forward scattered waves is slightly greater than the backward scattered waves for all the cases. For Cases 1 and 2, there does not seem to be any consistent trend in terms of delamination size. The amplitude of the second harmonic is not necessarily increasing with delamination size to the wavelength ratio. For Case 3, the amplitudes of the forward and the backward scattered waves seem to increase with delamination size, as shown in Fig. 15c. Therefore, the results indicate that the amplitude of second harmonic may not necessarily increase with delamination size. However, larger amplitude of second harmonic is observed when forward scattered wave signal is measured compared to backward scattered signal. This shows that forward scattered signals provide better information regarding existence of delamination in composite laminates than the backward scattered signals.

Fig. 8 Normalized amplitude of second harmonic against delamination size to the wavelength ratio for a) Damage Case 1 b) Damage Case 2 c) Damage Case 3

Effect of material damping and propagation distance

In this section the effect of damping on interaction of A_0 guided wave with delamination due to CAN is studied. For this purpose, different Rayleigh damping values were considered in the FE models. The models were analysed using different Rayleigh damping values and the amplitude of second harmonic was captured and compared for all models. The mass proportional Rayleigh damping coefficient, α, has a small effect when excitation frequency is high. However, the frequency proportional Rayleigh damping coefficient, β, has a significant effect on the results. Therefore, α was considered constant in all models and β was varied from 1.128×10^{-15} to 1.128×10^{-6}.

The FE simulation results shown in Fig. 16 indicate that the amplitude of second harmonic decays with material damping. Here the results are for the wavelength to delamination ratio $d/\lambda = 1$ and three different through-thickness locations.

Fig. 9 Normalized amplitude of second harmonic as a function of Rayleigh damping value for delamination of $d/\lambda = 1$ for incident wave being centered around 140 KHz.

The results indicate that amplitude of second harmonic decreases rapidly with damping when the Rayleigh damping coefficient exceeds 1.128×10^{-8} which is the Rayleigh damping coefficient corresponding to the incident wave. Considering that the Rayleigh

damping coefficient for the present composite material is 1.128×10^{-8} rad/s at 140 KHz and the frequency proportional damping coefficient is inversely proportional to the square of frequency (Eq. 5), frequency has a significant influence on nonlinear wave amplitude.

In addition to the effect of material damping on the magnitude of second harmonic, the propagation distance also has a major effect on the magnitude of nonlinear waves. The data was captured at several measurement points for backward and forward scattered waves and processed in the frequency domain. Measurement points were located at 5λ ($\lambda = 8\,mm$) from the centre of delamination and at a spacing of 10 mm (1.25 λ) between each other. The captured data at each measurement point were normalized to the amplitude of incident wave at the same measurement points in intact model.

The FE simulation results indicate that the amplitude of the second harmonic decreases with propagation distance in both cases. Figs. 17 shows the normalized amplitude of second harmonic against propagation distance for delamination of d/λ =1 for all three different through-thickness locations. The results show that the second harmonic wave decreases exponentially with the propagation distance in the forward and backward scattering directions. Moreover, the Fig. 17 shows that the magnitudes of higher harmonic for all damage cases decay with the same slope for each case in forward and backward scattering direction. This means that larger amplitude of second harmonic may be obtained when measurement point is located closer to the delamination. Therefore, it is anticipated that better results are obtained when the measurement point is closer to the delamination.

Fig. 10 Normalized amplitude of second harmonic against propagation distance of forward and backward scattering waves for delamination of $d/\lambda = 1$

Effect of incident wave amplitude and number of cycles

To investigate the effects of the strength and length of tone burst on the nonlinear response, computational simulations were carried out by varying the peak amplitude and the number of cycles of the original tone burst wave. The data was captured for both forward and backward scattered waves. To investigate the effect of incident wave amplitude and the number of cycles on the second harmonic wave packet amplitude, the data from all damage cases were normalized to the maximum amplitude from the whole data set. FFT of the signal captured at measurement points for the reflected wave for Damage case 3 and $d/\lambda = 1$ was calculated. The results are presented in Figs.18a and 18b. Figs. 19a and 19b show the same results for transmitted waves. The results show that the amplitude of the second harmonic increases with incident wave amplitude and the number of cycle for both forward and backward scattered wave packets. However, the ratio of the amplitude of second harmonic to the incident wave amplitude remains constant for all cases. Since the proposed damage detection technique relies on the amplitude of the higher harmonics wave packets, the results indicate that using larger tone burst wave amplitude and greater number of cycle will result in better damage detection outcome.

Fig. 11 FFT of normalized reflected wave for various incident wave magnitudes and lengths – Damage case 3 and $d/\lambda = 1$

Fig. 12 FFT of normalized transmitted wave for various incident wave magnitudes and lengths – Damage case 3 and $d/\lambda = 1$

Conclusions

The generation and propagation of nonlinear wave by the interaction symmetric (A_0) guided wave with the delamination in a composite laminate has been investigated using experimentally validated 3D finite element simulations. The focus of the study is on the effects of delamination size and through-thickness delamination location on the higher harmonics. By accounting the surface contact and material damping, the FE model is able to provide a reasonable prediction of the linear and nonlinear guided wave due to a delamination crack in fibre reinforced laminated composite beams. The higher harmonic induced by the interaction of the incident A_0 guided wave with the delamination has been extracted and analysed in frequency domain and time-frequency domain using FFT and wavelet transform.

The results of FE simulation of the composite beam with a delamination show that higher harmonics of guided waves are generated due to the clapping motion at the delamination region. The magnitude of the higher harmonic wave depends on the through-thickness location of the delamination but a delamination at the mid-plane of the beam generating almost no detectable higher harmonics. The higher harmonic waves are observed in both forward and backward scattering signals.

The existence of higher harmonics is a good indication for contact type of defects in laminated composite beams and can be utilized for detecting delamination in composite laminates. The second harmonic exhibits a larger magnitude in forward scattering

direction than backward scattering direction. Therefore, it has an advantage in monitoring the higher harmonic waves at the forward scattering direction. Moreover, it was shown that the generation of higher harmonics is influenced by through thickness location of delamination and varies for each damage case.

The studies on material damping and propagation distance indicate that the amplitude of second harmonic decreases when damping and propagation distance increase. This is very important as longer propagation distance may result in smaller amplitude of higher harmonics, which makes the damage detection more difficult and inefficient. It is also anticipated that damage detection becomes more complicated when material damping is high. The results of this study have shown an exponential decrease in second harmonic amplitude with increasing material damping. Therefore, the measurement location and material damping are two important key factors for using second harmonic generated by CAN in damage detection.

The results of computational models with different tone burst wave amplitude and the number of cycle indicate that the amplitude of second harmonic wave packet increases with the amplitude and the number of cycles of the incident tone burst. Therefore, larger tone burst wave amplitude and greater number of cycle should be considered as two important factors during the damage detection.

The results also show that processed data in frequency domain provide more information regarding delamination in composite beams as the time domain data provide little information. Therefore, frequency domain data are more reliable for damage detection.

Overall this study has provided new insights into the phenomenon of second harmonic generated by CAN at delamination in laminated composites. The characteristics of the nonlinear forward and backward scattering wave have been studied in detail. The findings of this study can be used to validate and improve the performance of damage detection methods using nonlinear guided wave.

Acknowledgements

This work was supported by the Australian Research Council under Grant Number DE130100261 and DP160102233. Eugene Chan from RMIT University contributed the manufacturing of the laminated composite beam specimens. The supports are greatly appreciated.

References

1. Achenbach JD. Quantitative non-destructive evaluation. *Int J Solids Struct* 2000; 37: 13-27.
2. Rose JL. A baseline and vision of ultrasonic guided wave inspection potential. *J Press Vess* 2002; 124: 273-282.
3. Raghavan A and Cesnik CES. Review of guided-wave structural health monitoring. *Shock Vib. Digest* 2007; 39: 91-114.
4. Veidt M, Ng CT, Hames S and Wattinger T. Imaging laminar damage in plates using Lamb wave beamforming. *Adv Mater Res* 2008; 47-50: 666-669.
5. An YK and Sohn H. Integrated impedance and guided wave based damage detection. *Mech Sys Sig Process* 2012; 28: 50-62.

6. Ng CT. Bayesian model updating approach for experimental identification of damage in beams using guided waves. *Struct Health Monitor* 2014; 13: 359-373.
7. Haynes C and Todd M. Enhanced damage localization for complex structures through statistical modelling and sensor fusion, *Mech Syst Sig Process* 2015; 54-55: 195-209.
8. Ng CT. A two-stage approach for quantitative damage imaging in metallic plates using Lamb waves. *Earthquake Struct* 2015; 8: 821-841.
9. Wandowski T, Malinowski PH. and Ostachowicz WM. Circular sensing networks for guided waves based structural health monitoring. *Mech Syst Sig Process* 2016; 66-67: 248-267.
10. Wang C.H. and Chang F.K. Scattering of plate waves by a cylindrical inhomogeneity. *Journal of Sound and Vibration 2005*: **282**: 429-451
11. Soleimanpour Reza and Ng CT. Mode conversion and scattering analysis of guided waves at delaminations in laminated composite beams. *Journal of Structural Monitoring and Maintenance 2015*:2:3: 213-236.
12. Klepka A., Staszewski W.J., Jenal R.B., Szwedo M., Iwaniec J., Uhl T., 2011, Nonlinear acoustics for fatigue crack detection – experimental investigations of vibro-acoustic wave modulations. *Structural Health Monitoring* 2011, 11:2: 197-211.
13. Liu Y, Kim, JY, Jacobs LJ, Qu J and Li Z. Experimental investigation of symmetry properties of second harmonic Lamb waves. *J. Appl. Phys* 2012; 111:053511-053511.

14. Kim J, Jacobs L and Qu J. Experimental characterization of fatigue damage in a nickel-base superalloy using nonlinear ultrasonic waves. *J Acoust Soc Am* 2006; 120: 1266-1273.
15. Deng M. Cumulative second-harmonic generation accompanying nonlinear shear horizontal mode propagation in a solid plate. *J Appl Phys* 1998; 84(7): 3500–3505.
16. Deng M. Cumulative second-harmonic generation of Lamb-mode propagation in a solid plate. *J Appl Phys* 1999; 85(6): 3051–3058.
17. Müller MF, Kim JY and Qu J, et al. Characteristics of second harmonic generation of Lamb waves in nonlinear elastic plates. *J Acoust Soc Am* 2010; 127(4): 2141–2152.
18. Zhang Z, Liu D, Deng M, Ta D and Wang W. Experimental observation of cumulative second-harmonic generation of lamb waves propagating in long bones. *Ultrasound Med Bio* 2014; 40: 1660-1670.
19. Xiang Y, Deng M, Xuan FZ and Liu CJ. Effect of precipitate dislocation interactions on generation of nonlinear Lamb waves in creep damaged metallic alloys. *J Appl Phys* 2012; 111:104905.
20. Lissenden C. J, Liu Y, Choi G. W, Yao X. Effect of Localized Plastic Deformation on Higher Harmonic Guided Wave Mode Generation in Plate. *J Nondestruct Eval* 2014; 33:178–186
21. Pruell C, Kim JY, Qu J and Jacobs LJ. Evaluation of fatigue damage using nonlinear guided waves. *Smart Mater Struct* 2009; 18: 035003.
22. Bermes C, Kim J and Qu J. Experimental characterization of material nonlinearity using Lamb waves. *App Phys Let* 2007; 90(2):021901.

23. Srivastava A and Lanza di Scalea F. On the existence of antisymmetric or symmetric Lamb waves at nonlinear higher harmonics. *J Sound Vib* 2009: 323(3): 932–943.
24. Awrejcewicz J and Olejnik P. Friction Pair Modelling by a 2-DOF System; Numerical and Experimental Investigations. Proceedings of I. J. Bifurcation and Chaos 2005; 1931-1944.
25. Pecorari C and Solodov I. Non-classical Nonlinear Dynamics of Solid Interfaces in Partial Contact for NDE Applications. Springer Journals 2006; 307-324.
26. Nazarov VE and Sutin A. Nonlinear Elastic Contacts of Solids with Cracks. J Acoust Soc Am 1997; 102: 3349-3354.
27. Kishiwada S, Biwa S, Inserra C and Matsumoto E. Modelling of flexural wave propagation in a plate with contacting interface. Proceeding of Asian pacific conference for materials and mechanics 2009; 2368-2372.
28. Kim N, Lee TH, Jhang KY and Park IK. Nonlinear Behaviour of Ultrasonic Wave at Crack. AIP Conf 2010; 1211: 73.
29. Hong M, Su Z, Wang Q, Cheng L and Qing X. Modelling nonlinearities of ultrasonic waves for fatigue damage characterization. Ultrasonics 2014; 54: 770-778.
30. Solodov I. Wackerl J, Pfleiderer K and Busse G. Nonlinear self-modulation and subharmonic acoustic spectroscopy for damage detection and location. Appl Phys Lett 2004; 84(N26) 5386-5388.
31. Kishiwada S, Biwa S, Inserra I, Matsumoto E. Nonlinear Ultrasonic Characterization of Lamb Wave in a Plate with Contacting Interfaces. *Proceedings of ICCAS-SICE* 2009; *2368*: 1-6.

32. Korotkov AS, Slavinsky MM and Sutin AM. Variations of acoustic nonlinear parameters with the concentration of defects in steel. *J Acoust Phys* 1994; 40: 71-74
33. Donskoy A, Sutin A and Ekimov C. Nonlinear Acoustic Interaction on Contact Interfaces and its use for Nondestructive Testing. *NDT & E Int* 2001; 34: 231-238.
34. Li, W, Cho, Y, Achenbach J. D. Detection of thermal fatigue in composites by second harmonic Lamb waves. *Smart Materials and Structures* 2012; 21:8: 085019.
35. Zhao, J, Chillara V. K, Ren B, Cho H, Qiu J, Lissenden, C. J. Second harmonic generation in composites: Theoretical and numerical analyses. *Journal of Applied Physics* 2016; 119:6:064902.
36. Castaings M and Hosten B. Lamb and SH waves generated and detected by air-coupled ultrasonic transducers in composite material plates. *NDT & E Int* 2001; 34: 249-258.
37. Ng CT. On the selection of advanced signal processing techniques for guided wave identification using a statistical approach. *Eng Struct* 2014; 67: 50-60.
38. Ramadas C, Balasubramaniam K, Hood A, Joshi M and Krishnamurthy CV. Modelling of attenuation of Lamb waves using Rayleigh damping: Numerical and experimental studies. *Composite Struct* 2011; 93: 2020–2025.
39. Ng CT. On accuracy of analytical modelling of Lamb wave scattering at delaminations in multilayered isotropic plates. *Int J Struct Stab Dyn* 2015; 15(1540010): 1-12.
40. Packo P, Uhl T, Staszewski W.J. Generalized semi-analytical finite difference method for dispersion curves calculation and numerical dispersion analysis for Lamb waves. *J. Acoust. Soc. Am.* 2014;136 :3:993-1002.

41. Zhao J., Chillara V. K., Ren B, Cho H., Qiu J., Lissenden, C. J. Second harmonic generation in composites: Theoretical and numerical analyses. *Journal of Applied Physics* 2016;119(6): 064902.
42. Ng C. T, Veidt M. A Lamb-wave-based technique for damage detection in composite laminates. *Smart Mater. Struct* 2009;18: 1–12.
43. Maio L, Memmolo V, Ricci F, Boffa N.D, Monaco E, Pecora, R. Ultrasonic wave propagation in composite laminates by numerical simulation. *Composite Structures* 2015;121:64–74.
44. Stewart JR, Gullerud AS, Heinstein MW, Solution verification for explicit transient dynamics problems in the presence of hourglass and contact forces. *J Comp Methods App Mech Eng* 2006; 195: 1499–1516.
45. Ng CT, Veidt M and Rajic N. Integrated piezoceramic transducers for imaging damage in composite laminate. *Proceedings of SPIE* 2009; *7493*: 1-8.
46. He S and Ng CT. Analysis of mode conversion and scattering of guided waves at cracks in isotropic beams using a time-domain spectral finite element method. *Elect J Struct Eng* 2015; 14: 20-32.
47. ABAQUS Theory Manual Version 6.9, 2009, ABAQUS Inc.
48. Stepinski, Tadeusz, Uhl , Tadeusz, Staszewski , Wieslaw, Advanced Structural Damage Detection : From Theory to Engineering Applications, Wiley, 2003
49. Kovic B and Lowe M. DISPERSE User's Manual Version 2.0.16B. *Imperial College. University of London, Non-Destructive Testing Laboratory* 2003.

Tables

Table 1: Elastic properties of the VTM264 prepreg lamina

E_{11} (GPa)	E_{22} (GPa)	E_{33} (GPa)	G_{11} (GPa)	G_{12} (GPa)	G_{13} (GPa)	$\boldsymbol{v_{12}}$	$\boldsymbol{v_{13}}$	$\boldsymbol{v_{23}}$
120.20	7.47	7.47	3.94	3.94	2.31	0.32	0.32	0.33

Table 2: Damage cases according to delamination size to wavelength ratio (d/λ)

d/λ	0.50	0.75	1.00	1.25	1.50	1.75	2.00
Delamination size (mm)	4	6	8	10	12	14	16

Table 3: Damage cases with different through-thickness locations of delamination

Damage case	1	2	3	4
Delamination through-thickness location	Between 1st & 2nd layers	Between 2nd & 3rd layers	Between 3rd & 4th layers	Between 4th & 5th layers

Figures

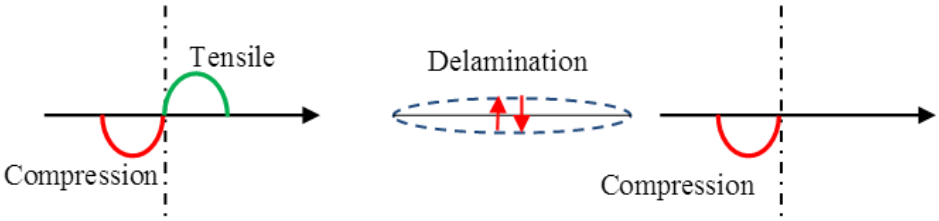

Fig.13 Interaction of an incident wave with a crack

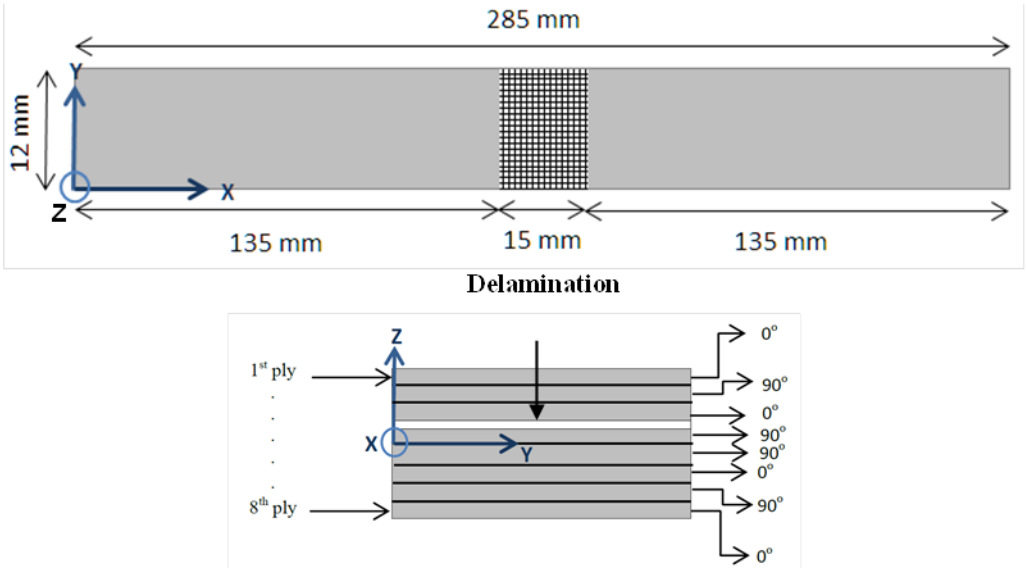

Fig. 14 Schematic diagram of a composite beam specimen with delamination and its cross section

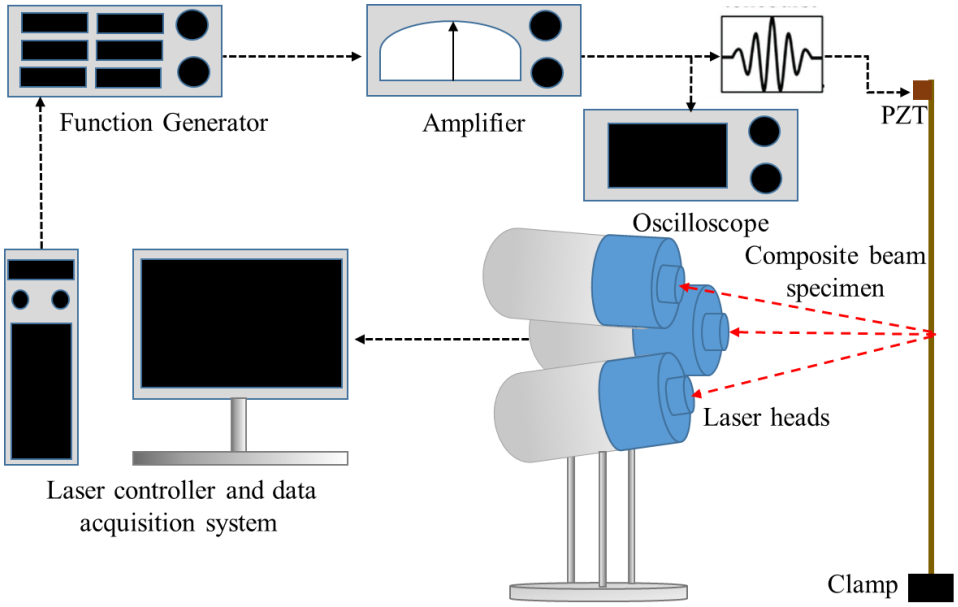

Fig. 15 Experiment setup used for verification of FE models

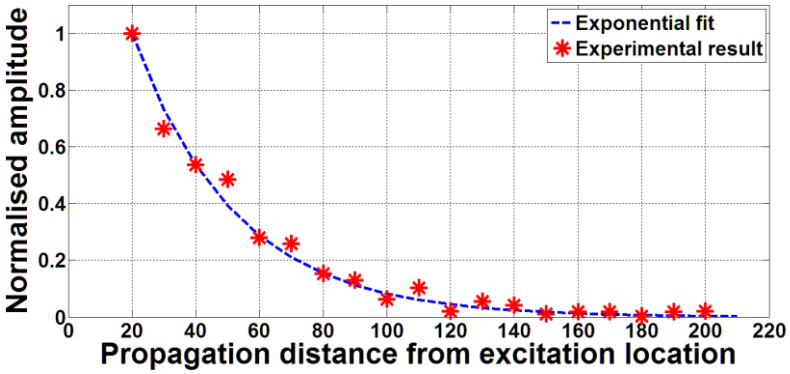

Fig. 16 Attenuation of A_0 guided wave in composite structure at 140 kHz

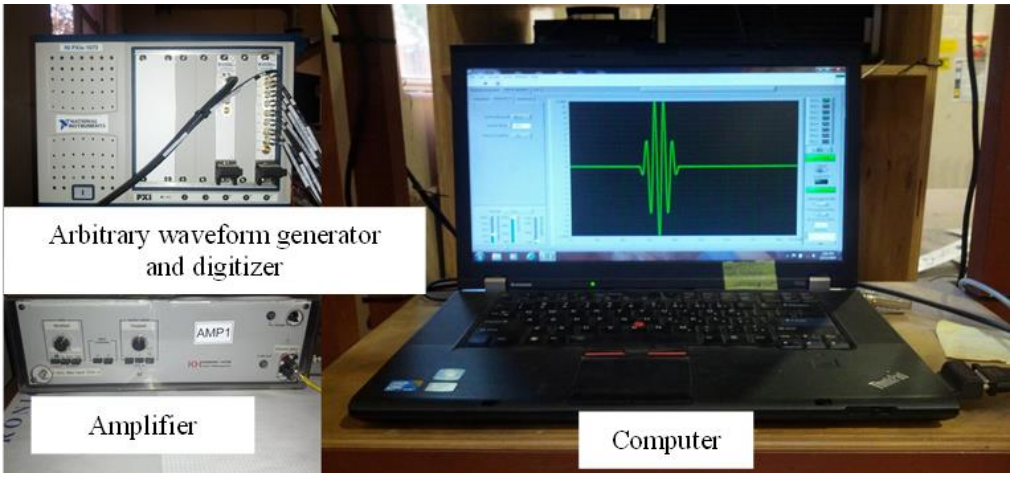

Fig. 17 Excitation and acquisition of higher harmonic waves

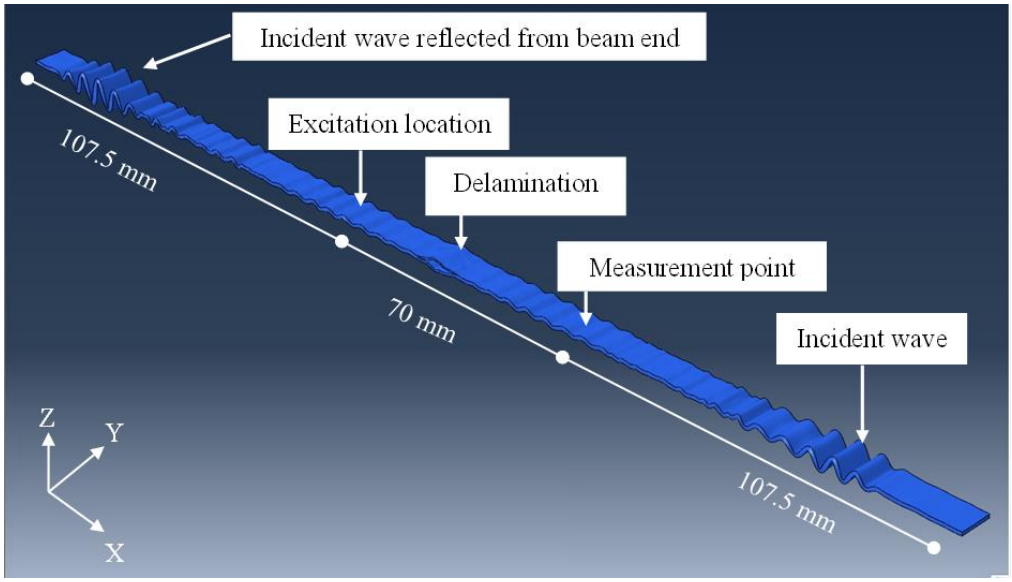

Fig. 18 A typical contour snapshot of FE simulated out-of-plane displacement of guided wave in composite beam with a delamination (time = 128.9 μs. Scale factor = 250)

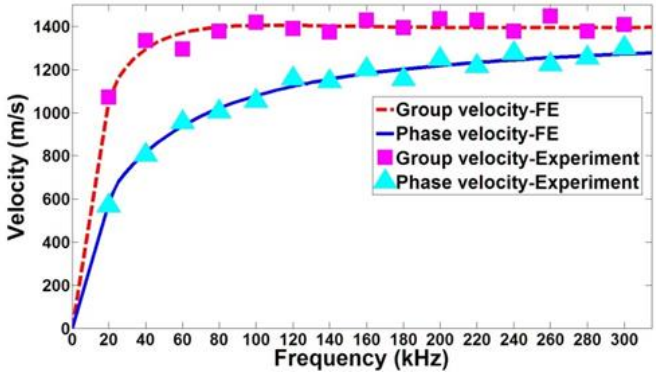

Fig 7. Dispersion curve comparison estimated by FE and experimental results

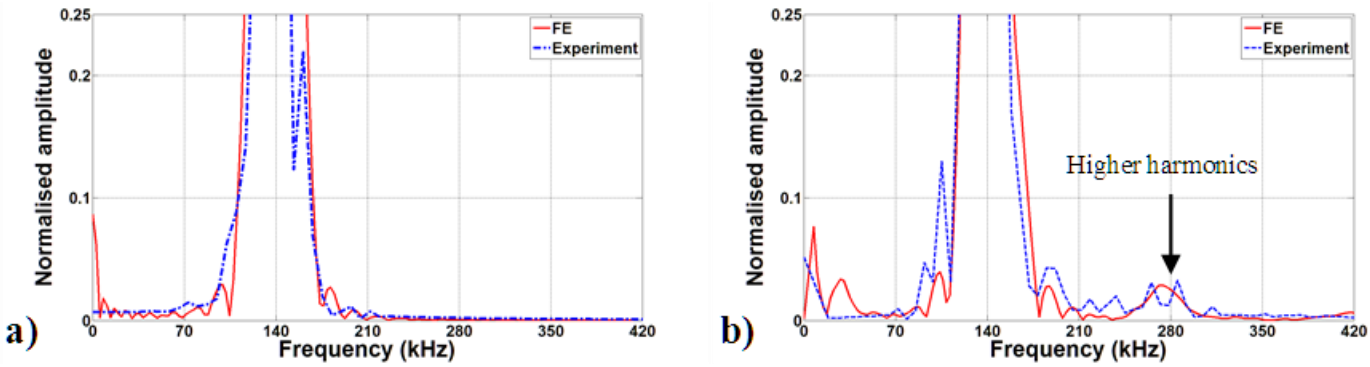

Fig. 8 Normalized FFT of the signal obtained from the experiment and FE simulation, a) intact beam b) beam with the delamination between 3rd and 4th ply. The response measured at 70 mm from excitation and 35 mm from centre of delamination.

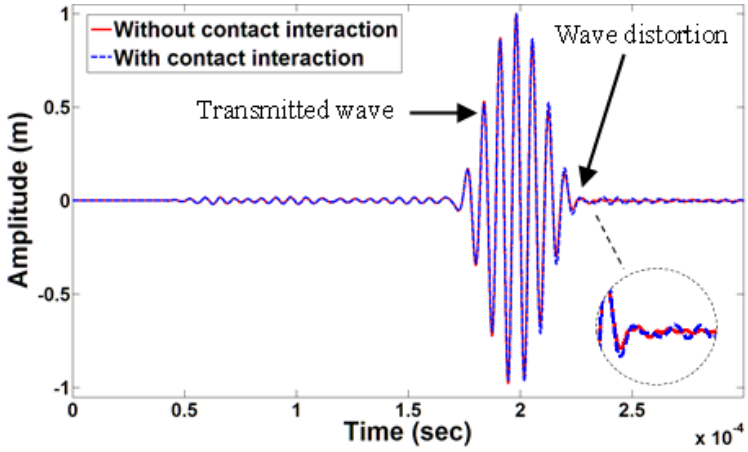

Fig. 9 Transmitted wave response computed by finite element model for damage case study 3, $d/\lambda = 1$

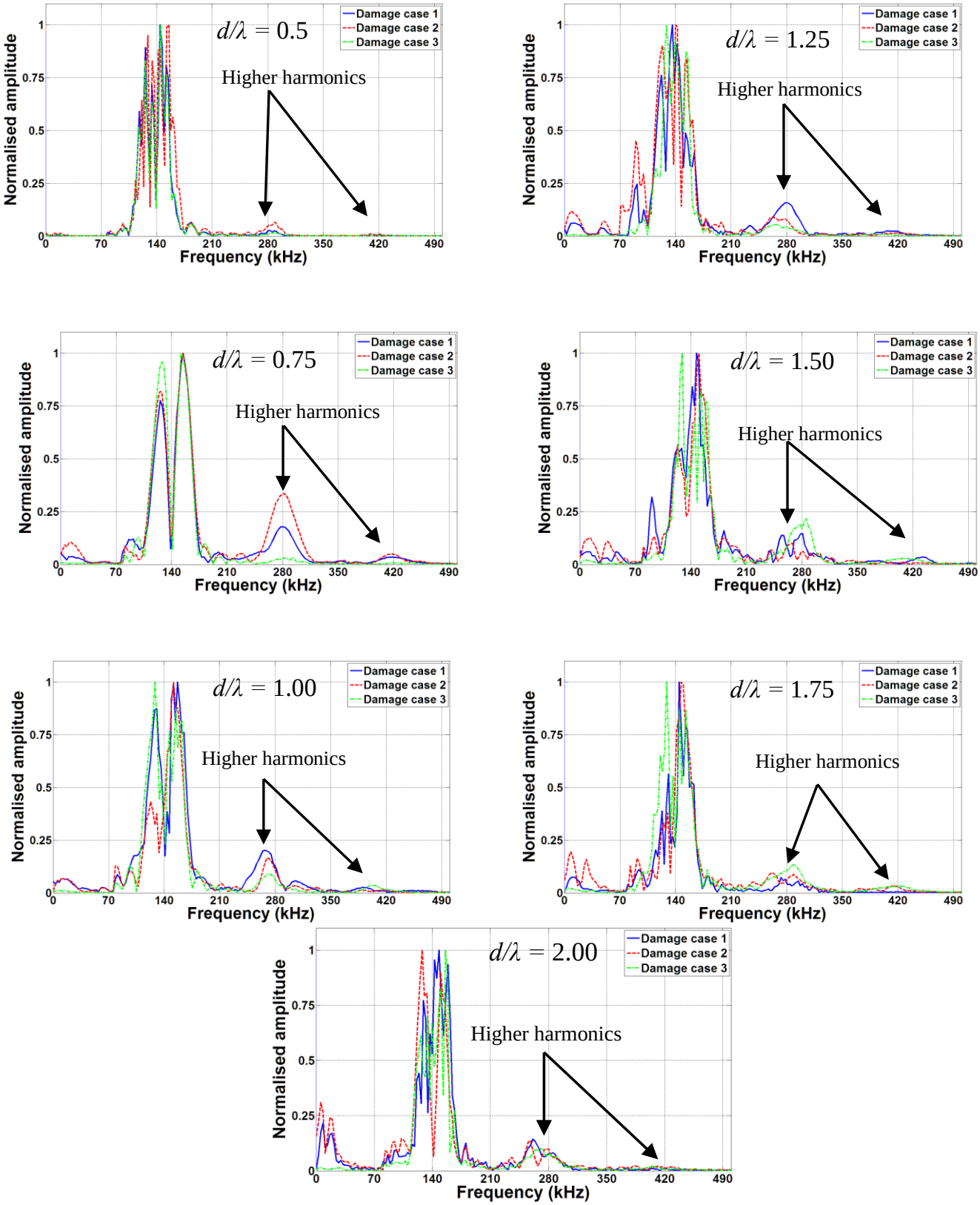

Fig. 10 FFT of forward scattered wave by using baseline subtraction

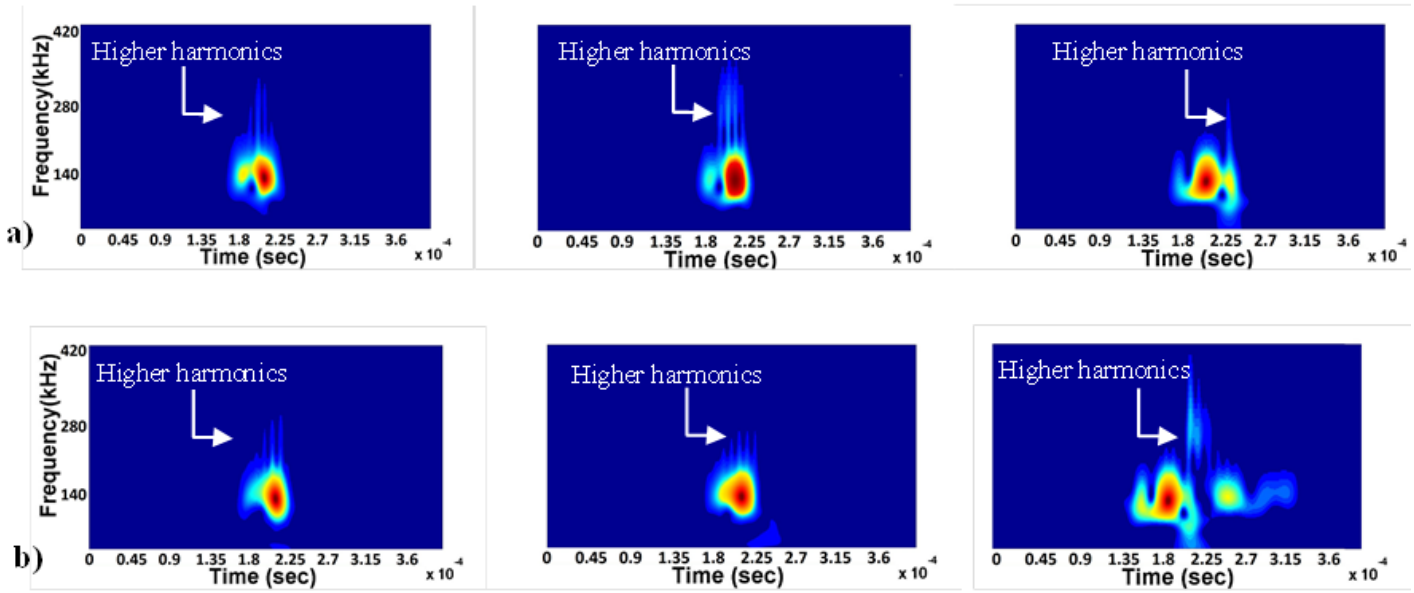

Fig. 19 Time-frequency energy density spectrum of forward scattered wave by using baseline subtraction

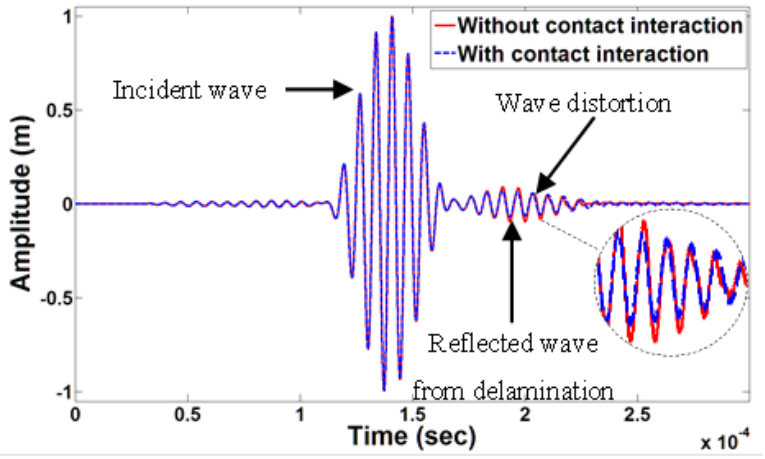

Fig. 20 Reflected waves of Damage Case 3 (d/λ= 1) from FE models.

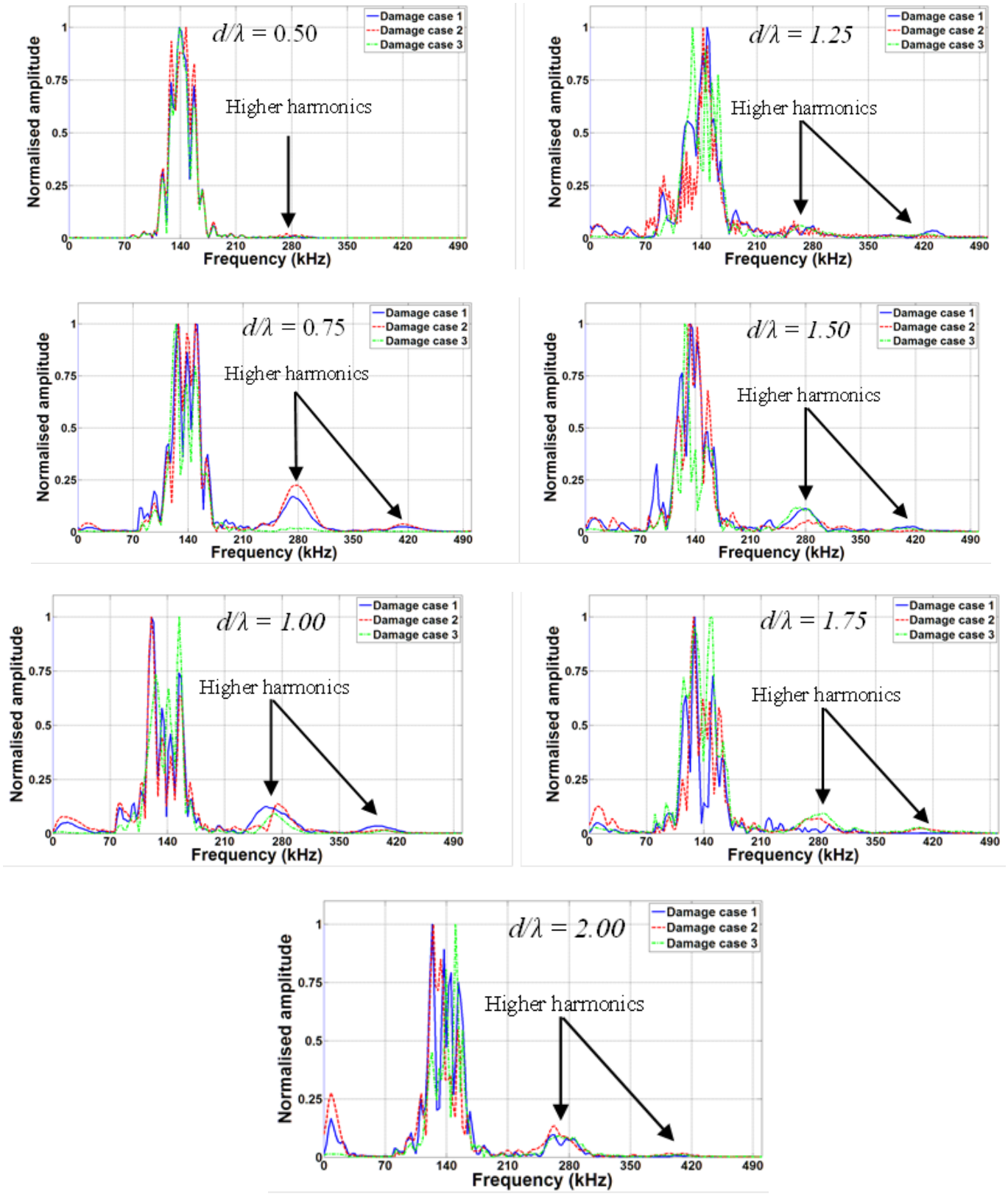

Fig. 13 FFT of nonlinear backward scattering waves extracted using baseline subtraction

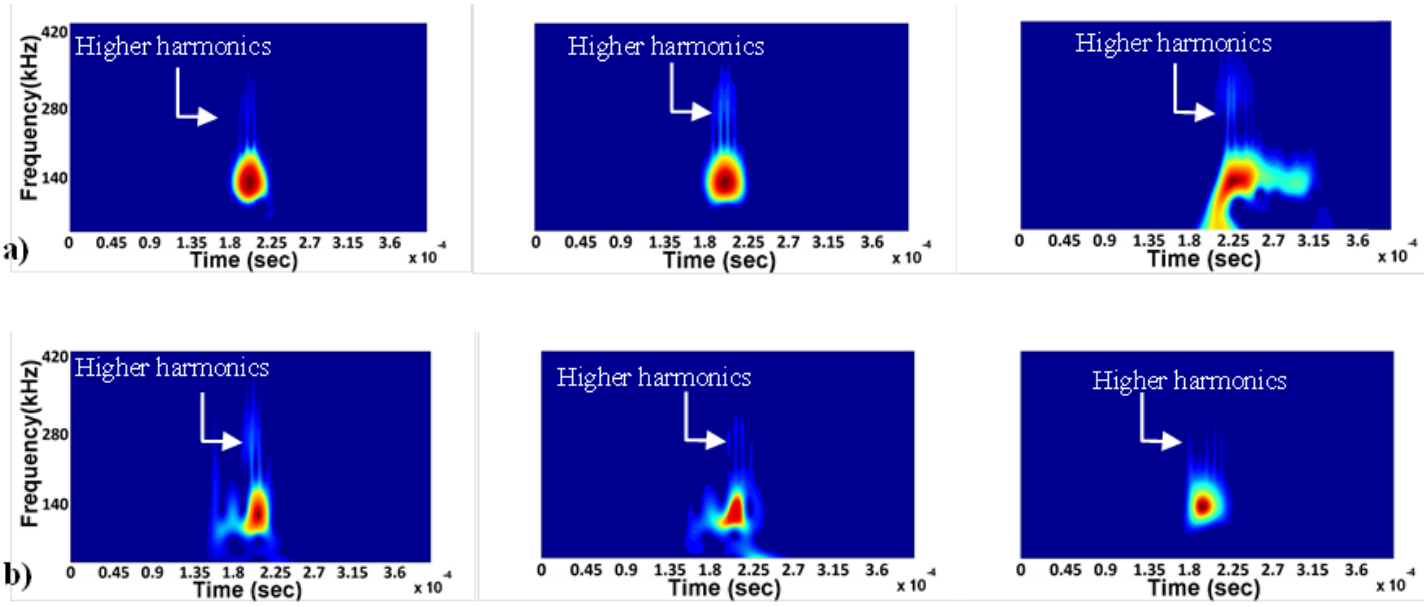

Fig. 14 Time-frequency energy density spectrum of backward scattered wave (after baseline subtraction) for Damage Cases 1-3 (left to right) and delamination size to the wavelength ratio of a) 0.75 and b) 1

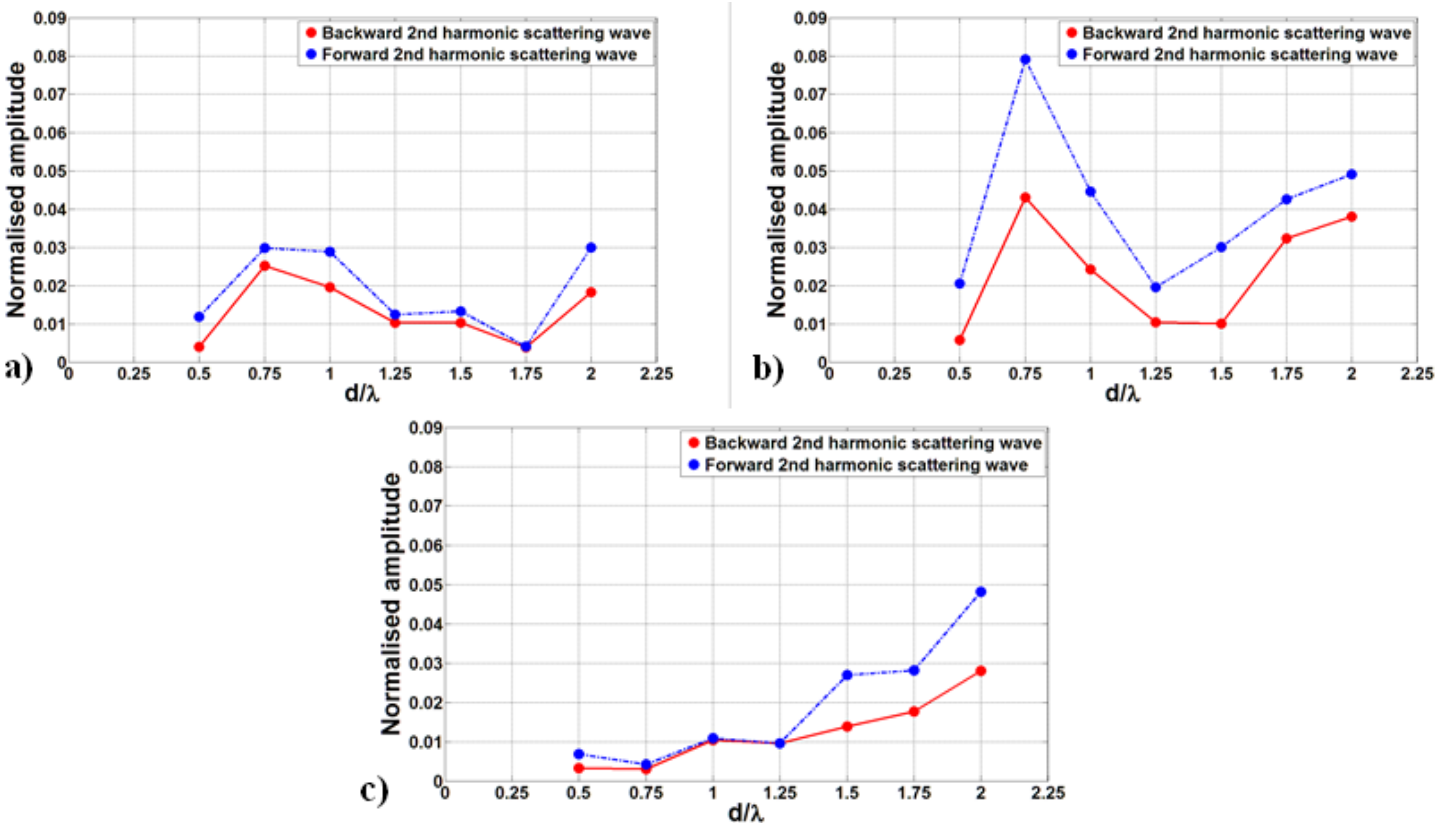

Fig. 21 Normalized amplitude of second harmonic against delamination size to the wavelength ratio for a) Damage Case 1 b) Damage Case 2 c) Damage Case 3

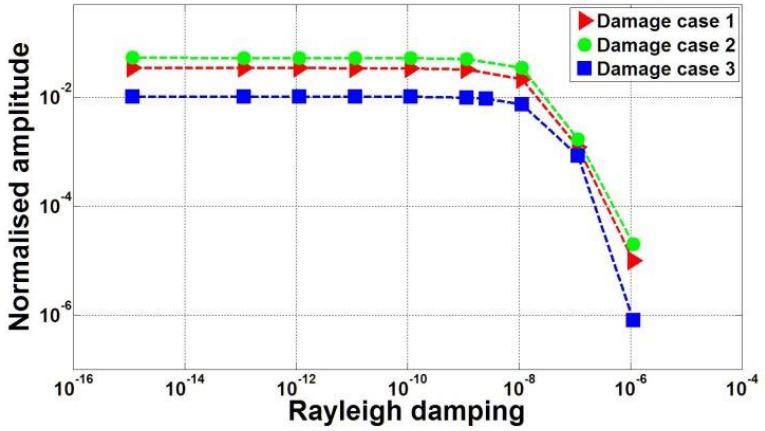

Fig. 22 Normalized amplitude of second harmonic as a function of Rayleigh damping value for delamination of d/ λ = 1 for incident wave being centered around 140 KHz.

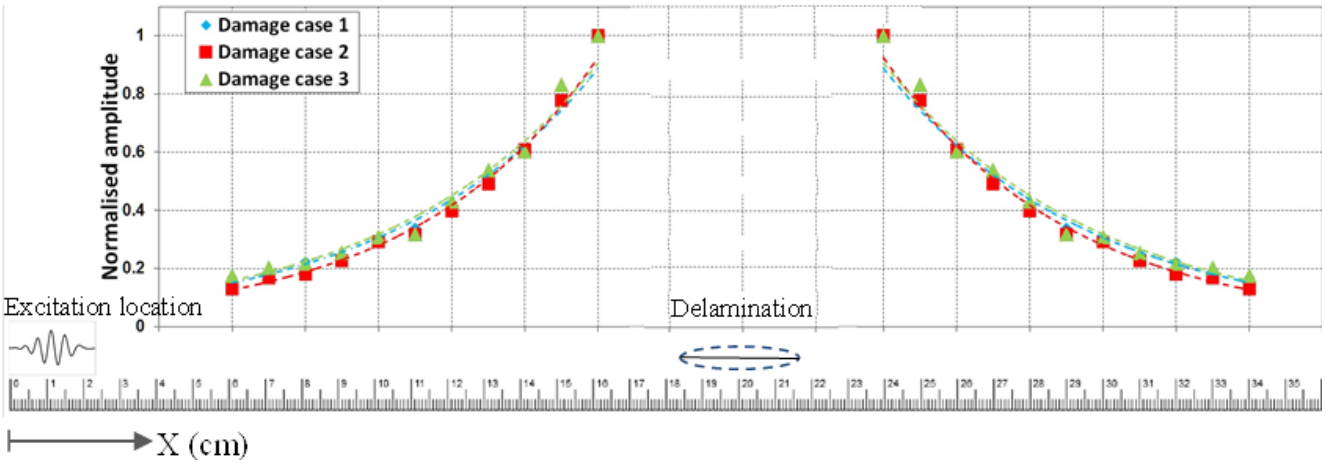

Fig. 23 Normalized amplitude of second harmonic against propagation distance of forward and backward scattering waves for delamination of $d/\lambda = 1$

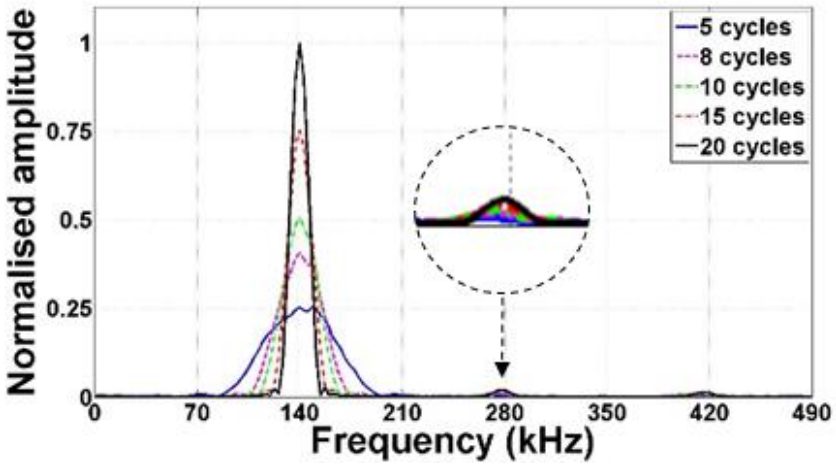

(a) Tone burst pulse with different number of cycles

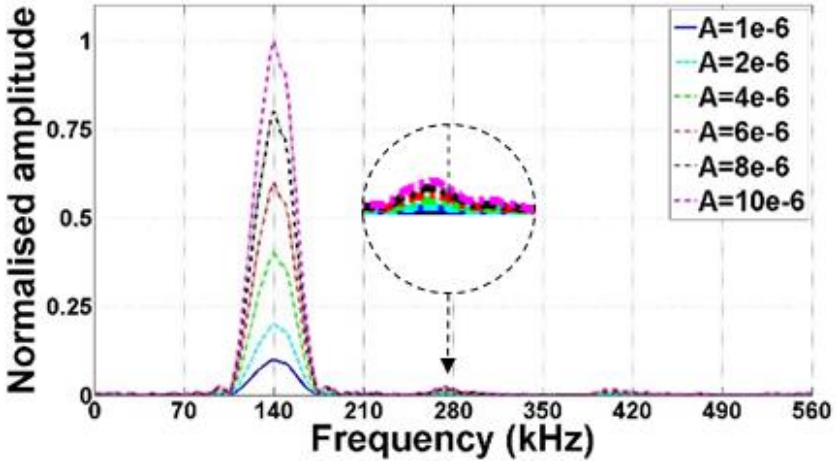

(b) Different incident wave amplitudes

Fig. 24 FFT of normalized reflected wave for various incident wave magnitudes and lengths – Damage case 3 and $d/\lambda = 1$

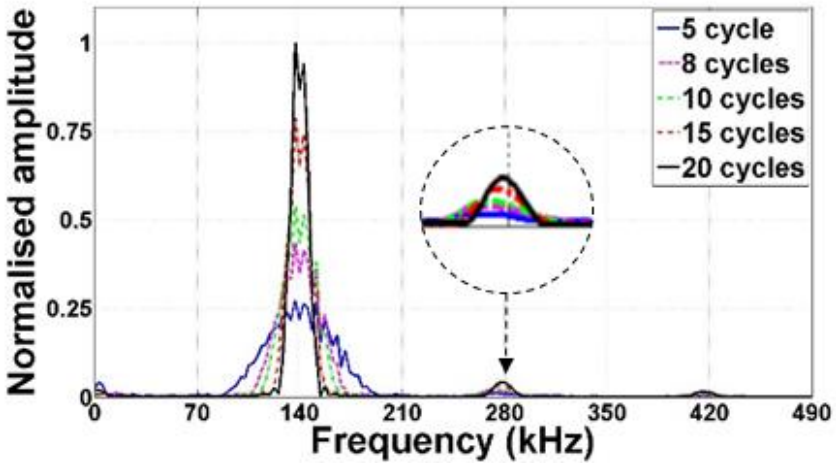

(a) Tone burst pulse with different number of cycles

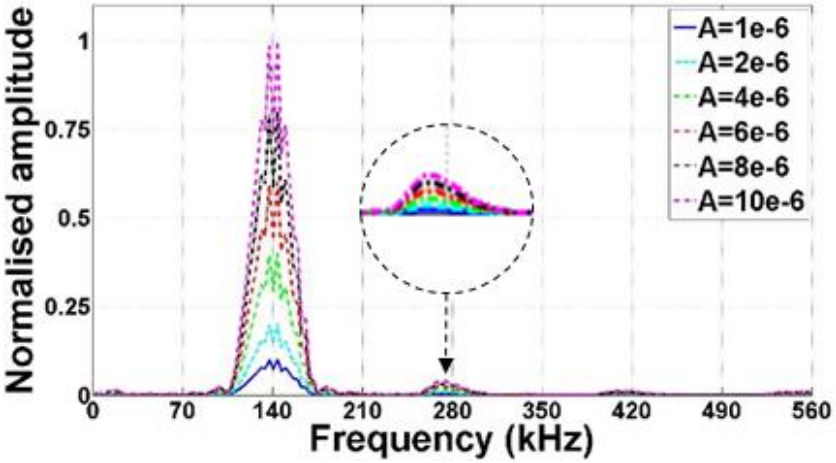

(b) Different incident wave amplitudes

Fig. 25 FFT of normalized transmitted wave for various incident wave magnitudes and lengths – Damage case 3 and $d/\lambda = 1$